The Development of a Methodology to Scale Between Cold-Flow and Hot-Fire Evaluations of Gas-Centered Swirl Coaxial Injectors

P.A. Strakey, R.K. Cohn, and D.G. Talley
Air Force Research Laboratory, Edwards AFB, CA

ABSTRACT

Uni-element cold flow and hot fire evaluations were performed on a variety of gas-centered swirl coaxial injectors. Gaseous oxygen and various liquid hydrocarbons were used in the combustion evaluations, while water and gaseous nitrogen were the simulants for the cold flow experiments. The connections between the two sets of data were examined.

The cold flow experiments demonstrated that the mixing efficiency of the various injector designs was highly sensitive to the internal geometry of the injector as well as the scaling methodology used to simulate the hot-fire conditions. When the proper scaling methodology was employed, a correlation which captures the general trend of injector geometry and c* performance between the measured cold-flow mixing efficiency and hot-fire c* performance was observed. This semi-empirical correlation was developed based on a film stripping mechanism that relates the measured c* efficiency of these injectors to the injector geometry and fuel properties. The effects of injector geometry on the injector internal flowfield were ascertained with a combination of cold-flow CFD simulations and experimental measurements.

The correlation also implies that fuel properties are secondary to injector geometry effects in determining the performance of various injector configurations. Hot-fire testing of several common hydrocarbon fuels including RP-1, Butane, JP-10, JP-7 and JP-8 confirmed that injector geometric effects dominated performance and demonstrated that c* efficiency in excess of 95% is achievable with all of these fuels. However, the effect of fuel properties does appear to be within the measurement limits of the experiments and a correlating parameter which captures these effects was found.

INTRODUCTION

The development of a liquid rocket engine is an arduous task typically involving extensive testing at both large and small scales. Since testing at large scales is extremely expensive, it is of interest to understand how modeling and simulation and inexpensive cold flow and hot fire evaluations on a uni-element scale can best be combined to advance the injector design before committing to larger scales. In addition to being inexpensive, evaluations on a uni-element scale are often capable of producing a large amount of information within a short period of time. Accordingly, it was decided to develop such an understanding of scaling for the gas-centered swirl coaxial class of injectors. An oxygen-rich staged combustion liquid hydrocarbon engine was selected as the baseline cycle.

A reasonable design principle for coaxial injectors is to attempt to shroud the oxidizer in the central flow with the fuel as the annular flow. The goal is for the oxidizer to be completely encapsulated and consumed by the fuel, thus preventing it from reaching the combustion chamber walls. In some applications, the oxidizer injected into the main combustion chamber is a liquid, for example liquid oxygen, while the fuel is injected as a gas, for example gaseous hydrogen. In an oxygen-rich staged combustion liquid hydrocarbon engine, however, it would be the oxygen which is the gas and the fuel which is a liquid. This difference leads to fundamentally different injector designs. In the present study, a gas-centered swirl coaxial injector concept was selected, where swirl is imparted to the annular liquid fuel flow, while the central gaseous oxygen (GOX) flow is not swirled. Atomization of the fuel is accomplished through the development of surface instabilities on the liquid sheet by shear from the high-speed gas, which initiates ligamentation and ultimately atomization.

Design guidance in the US for liquid swirl-type injectors commonly comes from industrial applications that include industrial boilers, gas turbines, and spray drying. The guidance has been compiled in various monographs, such as refs. 1 and 2. However, these applications concern sprays which are introduced into a quiescent or co-flowing gas, with the gas typically being the oxidizer. These applications are more consistent with liquid-centered injectors. As such, this guidance is not directly applicable to gas-centered swirl coaxial injectors.

The following sections describe the injector designs, the cold flow uni-element test results and

_____

Report Documentation Page		*Form Approved* *OMB No. 0704-0188*	

Public reporting burden for the collection of information is estimated to average 1 hour per response, including the time for reviewing instructions, searching existing data sources, gathering and maintaining the data needed, and completing and reviewing the collection of information. Send comments regarding this burden estimate or any other aspect of this collection of information, including suggestions for reducing this burden, to Washington Headquarters Services, Directorate for Information Operations and Reports, 1215 Jefferson Davis Highway, Suite 1204, Arlington VA 22202-4302. Respondents should be aware that notwithstanding any other provision of law, no person shall be subject to a penalty for failing to comply with a collection of information if it does not display a currently valid OMB control number.

1. REPORT DATE **23 MAR 2004**	2. REPORT TYPE	3. DATES COVERED **-**

4. TITLE AND SUBTITLE **The Development of a Methodology to scale Between Cold-Flow and Hot-Fire Evaluations of Gas-Centered Swirl Coaxial Injectors**	5a. CONTRACT NUMBER
	5b. GRANT NUMBER
	5c. PROGRAM ELEMENT NUMBER
6. AUTHOR(S) **P Strakey; R Cohn; D Talley**	5d. PROJECT NUMBER **3058**
	5e. TASK NUMBER **RF9A**
	5f. WORK UNIT NUMBER

7. PERFORMING ORGANIZATION NAME(S) AND ADDRESS(ES) **Air Force Research Laboratory (AFMC),AFRL/PRS,5 Pollux Drive,Edwards AFB,CA,93524-7048**	8. PERFORMING ORGANIZATION REPORT NUMBER
9. SPONSORING/MONITORING AGENCY NAME(S) AND ADDRESS(ES)	10. SPONSOR/MONITOR'S ACRONYM(S)
	11. SPONSOR/MONITOR'S REPORT NUMBER(S)

12. DISTRIBUTION/AVAILABILITY STATEMENT **Approved for public release; distribution unlimited**

13. SUPPLEMENTARY NOTES

14. ABSTRACT

Uni-element cold flow and hot fire evaluations were performed on a variety of gas-centered swirl coaxial injectors. Gaseous oxygen and various liquid hydrocarbons were used in the combustion evaluations, while water and gaseous nitrogen were the simulants for the cold flow experiments. The connections between the two sets of data were examined. The cold flow experiments demonstrated that the mixing efficiency of the various injector designs was highly sensitive to the internal geometry of the injector as well as the scaling methodology used to simulate the hot-fire conditions. When the proper scaling methodology was employed, a correlation which captures the general trend of injector geometry and c* performance between the measured cold-flow mixing efficiency and hot-fire c* performance was observed. This semi-empirical correlation was developed based on a film stripping mechanism that relates the measured c* efficiency of these injectors to the injector geometry and fuel properties. The effects of injector geometry on the injector internal flowfield were ascertained with a combination of cold-flow CFD simulations and experimental measurements. The correlation also implies that fuel properties are secondary to injector geometry effects in determining the performance of various injector configurations. Hot-fire testing of several common hydrocarbon fuels including RP-1, Butane, JP-10, JP-7 and JP-8 confirmed that injector geometric effects dominated performance and demonstrated that c* efficiency in excess of 95% is achievable with all of these fuels. However, the effect of fuel properties does appear to be within the measurement limits of the experiments and a correlating parameter which captures these effects was found.

15. SUBJECT TERMS

16. SECURITY CLASSIFICATION OF:			17. LIMITATION OF ABSTRACT	18. NUMBER OF PAGES	19a. NAME OF RESPONSIBLE PERSON
a. REPORT **unclassified**	b. ABSTRACT **unclassified**	c. THIS PAGE **unclassified**		**19**	

CFD simulations, hot fire uni-element test results, and the connections found between these results. Combusting CFD calculations were also performed [3,4], but are not discussed here.

INJECTOR DESIGN

The basic gas-centered swirl coaxial element design can be conceptualized as a straight-run post for the gas. The post includes a discrete set of liquid injection orifices near the downstream exit of the gas post. The orifices are tangentially oriented to generate a swirling liquid film around the periphery of the element. The liquid film is thus subjected to a combination of cross-flow shear and centrifugal forces. The liquid is stripped from the film inside the element by the central gas jet, which entrains the droplets, transporting the resultant spray downstream. The parameters that can be varied in this design include the number of liquid injection orifices, the axial location of the orifices relative to the final injection location, and most importantly the post geometry near the liquid injection orifices. Three basic injector concepts were identified for comparative evaluation: diverging elements, converging elements, and pre-filming elements. These elements are shown schematically in Figure 1.

The diverging element design injects the fuel downstream of a sudden expansion, with the expansion having a characteristic expansion angle. A set of six parametric diverging elements was designed, as shown in Figure 1.

For the converging element, the liquid is injected tangentially into the outer annulus. Then, the outer annulus necks down to accelerate both the liquid and gaseous flows. Out of an initial set of four parametric converging element designs, one design was selected (#11) for evaluation.

The pre-filming element is an adaptation of designs commonly used in gas turbines and industrial boilers (1). The liquid is injected tangentially into a recessed groove (Fig. 1, #7 & #13). The axial dimension of the groove should be large enough to permit the liquid film to homogenize before being exposed to the high-speed gaseous core flow. The film is then circumferentially accelerated as the groove diameter narrows to the main gas port diameter. Two parametric pre-filming element designs were developed as shown in Figure 1.

COLD FLOW EVALUATIONS

Cold flow evaluations used water to simulate the liquid fuel and gaseous nitrogen to simulate GOX. The cold flow evaluations were performed in a vessel pressurized with gaseous nitrogen. The vessel design allows the back pressure to be adjusted and includes windows for optical access. The diagnostics utilized for this study included back-lit strobe imaging of the spray, mechanical patternation for measurement of liquid flux distribution and phase Doppler interferometry for droplet size and velocity measurement. The axial station for all diagnostics can be varied between 2.54 and 15.24 cm downstream of the injector exit, although most of the subject test data was collected at 5.08 cm.

The cold flow conditions were designed to simulate hot fire conditions with respect to propellant conditions at the point of injection. At the time of the cold flow evaluations, hot fire test pressures were projected to be 1.72 MPa (250 psia) and 3.44 MPa (500 psia) using butane as the fuel. The hot fire conditions were later extended both in pressure range and in the number of fuel types.

The cold flow injector operating conditions were designed to match to the hot fire operating condition in the following manner. First, the gas injection velocity was set to the corresponding hot fire operating velocity. Second, the injected gas density was matched to the hot fire density by setting the chamber back pressure. Since the density of nitrogen and oxygen at a given temperature and pressure are very similar, the second condition is achieved with only a slight variation in chamber back pressure relative to the hot fire chamber pressure. With oxidizer injection velocity and density equivalent to the hot fire case, the final adjustment was to match the hot fire gas-to-liquid momentum difference by adjusting the mass flow rate of liquid water. Using the above matching conditions, the injectors were tested at chamber pressures of 1.97 MPa (271 psig) and 3.93 MPa (556 psig), compared to 1.72 MPa (250 psia) and 3.44 MPa (500 psia) for the hot-fire conditions. Most of the cold-flow data presented here are for the 1.97 MPa (271 psig) condition. Higher pressure cold flow data is not presented due to dense spray effects which limited the ability to obtain optical diagnostic measurements. Selected elements were also tested over a range of injected mixture ratios. A comparison of the 1.72 MPa (250 psia) hot fire operating condition and the analogous cold flow simulation operating condition is included in Table 1.

Several different measurements were made of each element's performance characteristics, some qualitative and others quantitative. Back-lit strobe images were used to qualitatively compare the near-field spray patterns of the different injection

elements. Tests were run with only the liquid circuit operating and then with both fluid circuits operating. The "liquid only" tests produced a rapidly expanding liquid cone. The cone typically expanded with half-angles exceeding 75° and often wet the injector face plate. However, when the gas and liquid circuits were run simultaneously, the free liquid film was pulled inwards towards the gas core and rapidly entrained. The images for the 1481 N (333 lb$_f$) equivalent operating condition are presented in Figure 2. The largest angle diverging element (#3), appears to have the widest spray pattern with relatively large liquid droplets being thrown toward the periphery of the spray, while the other diverging elements (#5 and #12) show better entrainment of the liquid film into the gas flow. This is due to the higher gas velocity and improved liquid stripping of these designs.

The converging element (#11) produced a narrower spray cone with what appears to be finer droplet sizes. The large bore pre-filming element (#7) produced a well entrained spray but with a somewhat larger droplet size near the periphery of the spray, similar to element #5. The small bore pre-filming element (#13) produced a very narrow solid cone spray with excellent atomization.

More quantitative measurements were performed using a combination of mechanical patternation and phase Doppler velocimetry. In the mechanical patternation technique, the liquid (and gas) entering the mechanical patternator tubes drained into collection bottles where the liquid level was measured using a capacitance probe accurate to ± 2%. Although the gas vents off to a common manifold that connects back to the chamber, the pressure drop through the patternation system only allows about 25% of the gas to pass through the tubes. This generated a partial stagnation region at the entrance of the patternator tubes and prevented some of the smaller droplets from entering the tubes. The larger droplets have enough momentum to penetrate the stagnation zone and enter the tubes. The collection efficiency of the patternator was defined as the ratio of the integrated liquid mass flux to the injected liquid flow rate. The high gas flow rates and injection velocities generated by these swirl coaxial elements combined with the small droplet sizes resulted in measured collection efficiencies that were sometimes much less than 100%. The measured collection efficiencies were in the range of 60% - 100%.

Droplet size and velocity were measured using a phase Doppler interferometer. The instrument simultaneously measures the size and velocity of individual droplets as they pass through a 60 μm by 75 μm probe volume. The optical configuration in this experiment was set to measure droplet sizes ranging from 3.8 μm to 440 μm and velocities ranging from -50 m/s to 250 m/s. The average velocity of droplets less than 20 μm in diameter was taken as a good estimate of the average gas phase velocity (5). The extreme density of the spray prevented phase Doppler measurements at element flows above equivalent thrusts of 1481 N (333 lb$_f$). At this flow condition, data validation rates for droplet sizing were as low as 15% in the center of the spray, where the liquid mass flux was the highest. In comparison, data validation rates as high as 90% were achieved at the edges of the spray. The validation rates for the velocity measurements were much larger than those for the droplet sizing, typically greater than 97% throughout the spray.

In order to account for the low collection efficiency of the mechanical patternator, the raw liquid mass flux data were corrected by the measured collection efficiency for each radial profile. For example, if the collection efficiency was 80%, the liquid flux data were multiplied by a factor of 1.25. Radial profiles of liquid mass flux measured at 5.08 cm downstream of the injection point are displayed in Figure 3 for three of the injectors. The patternator collection efficiency is annotated on each plot. For each element, two radial slices oriented at right angles to one another apart were measured with the patternator to check for spray symmetry, they are denoted by the 90° and 0° markings. Most of the sprays appear to have a solid-cone structure when both the gas and liquid circuits are flowing. The diverging element (#3) generated a significantly wider spray pattern with only some of the liquid entrained into the central gas flow. Most of the liquid exited the injector in the form of a hollow cone as evidenced by the peaks in the liquid mass flux profiles at a radial location of 60 mm on each side of center (Fig. 3). This was also seen in the images in Fig. 2 The six other elements tested produced solid cone sprays with varying degrees of radial spreading.

Most of the mass flux patterns appeared to be well behaved, reaching a maximum value at the centerline and falling off with an approximately Gaussian distribution and good spray symmetry. One exception was the largest angle diverging element (#3) that showed a significant asymmetry in the liquid flux distribution. The extent of the asymmetry in the liquid flux profile of element #3 can be seen in Figure 3 for the two radial slices which are oriented 90° apart. The outboard peak in the liquid flux profile at 60 mm shifts from one side of the spray to the other. This type of behavior typically results in poor combustion performance.

The gas velocity profiles were all Gaussian-like in shape and were typical of simple turbulent jets. The mixture ratio distribution for each injector was calculated from the gas velocity and liquid flux profiles. The mixture ratio profiles provided an indication of the degree of mixing between the gas and liquid. An element with large deviations in mixture ratio from the average in regions where there is significant mass flow (such as #3) will result in poor combustion performance.

A more quantitative measure of mixture ratio uniformity that has commonly been used in the past is the Rupe mixing efficiency (6). The mixing efficiency is calculated by dividing the spray into a series of concentric rings or stream-tubes. Each ring has a measured liquid and gas mass flux. A modified version of the Rupe mixing efficiency was used here and is given by Equation 1.

$$E_m = 1 - \sum_{\substack{r_i<R}} m_{f_i}\frac{(R-r_i)}{R} - \sum_{\substack{r_i>R}} m_{f_i}\frac{(R-r_i)}{(R-1)}$$

$$r_i \equiv \frac{MR}{(1+MR)} \qquad R \equiv \frac{\overline{MR}}{(1+\overline{MR})} \qquad (1)$$

In eq. 1, m_{fi} is the mass fraction in each ring, and MR is the measured mixture ratio. The modification here is that the integrated liquid and gas flowrates are used instead of the injected flowrates. This is necessary because the integrated gas mass flowrate differs from the injected amount due to entrainment. The converging element design (#11) as well as the small bore diverging element (#12) and the pre-filming element (#13) all generated well mixed sprays with E_m on the order of 85% or better. Element #3 produced the poorest mixing with an E_m of only 30.4%, while element #5, with an E_m of 59.7%, and #7, with an E_m of 80.0%, were deemed to be of intermediate mixing. The element mixing is believed to play a direct role in combustion performance and will be discussed further in relation to the hot-fire results.

A comparison of the Sauter mean diameter for the six elements evaluated is provided in Figure 4. The Sauter mean diameter (SMD) was found to be inversely proportional to the gas velocity in the cup region, as would be expected. As the relative velocity between the liquid film and gas flow, and thus the Weber number, is increased, the shearing force on the liquid droplets also increases resulting in a smaller final drop size. Except for element #3 all of the elements provided good atomization with a SMD less than 75 μm.

The conclusions of the uni-element cold flow testing, which guided the selection of elements for the uni-element hot fire testing, were that the element designs which maintain high relative velocity between the gas and liquid film and allow sufficient residence time for liquid stripping and entrainment should perform the best. All of the element designs produced sprays that were hollow-cone with only the liquid flowing, but became solid-cone sprays with both the gas and liquid circuits flowing. Except for injector #3, the injection element concepts all produced sprays with adequate symmetry.

HOT FIRE TEST RESULTS

Hot fire evaluations were conducted using a copper heat-sink combustor with chamber lengths of 17.78 cm and 20.32 cm and a nominal contraction ratio of 25.2. Each test was several seconds in duration with at least a half-second of steady state operation. Details of the facility and the test hardware can be found in previous publications (7,8).

In excess of 1000 separate firings were conducted of the various elements. Chamber pressures have ranged from 1.37 MPa (200 psia) to in excess of 6.87 MPa (1000 psia). Two series of evaluations were conducted. First, butane and RP-1 fuels were evaluated for a variety of injector geometries. Then, a variety of fuels were evaluated using one of the injector designs (#11). This was motivated by a need to validate the capability of the facility to make measurements of the required accuracy, and by the expectation that was developed during the progress of this study that the performance of injector #11 should be relatively insensitive to the identity of the fuel. Injector #11 also demonstrated low combustion noise characteristics.

The metrics used to characterize the hot fire data include characteristic velocity (c*), heat load, and chug stability. The c* efficiency measurements assume the ideal c* can be calculated using the CEA chemical equilibrium code assuming a finite area combustor. Heat loss to the walls and other losses are neglected. Despite this, it is reasonable to assume that these losses will be similar between the different injector types, thus allowing for comparisons between the elements.

Propellant flow rates were measured with cavitating venturis and sonic nozzles. The liquid venturis were calibrated with water, RP-1, and JP-10. The calibrations were then compared with each other, after correcting for vapor pressure and density. Typically, these three calibrations agreed to within 1%.

4

The sonic nozzles were also calibrated using GN2 to develop the appropriate discharge coefficient for the nozzle. Spot-check calibrations with GOX provided suitable confidence in these results. Uncertainty estimates for the liquid venturi flow rates are less than 1%. Primarily, this uncertainty is the result of the process of converting results between the different fluid media. Estimate for the gas-side flow rate uncertainty is 0.5%. Both of these values can be reduced by performing all calibrations with the requisite propellant.

The chamber pressure transducers used for these experiments were accurate to 0.05% of their full-scale value. Since measurements were typically made at ¼ of their full-scale output, the typical pressure measurement uncertainty is 0.20%. Another significant player in the uncertainty is the nozzle diameter. Combined in this uncertainty are the accuracy of the measurement of the nozzle as well as the change in the nozzle diameter as it heats during the test. It is estimated that this error is less than 0.05 mm. Using the nominal nozzle diameter of 1.14 cm, this yields an uncertainty of 0.44%.

Using these values the estimated uncertainty in the c* measurements is +/-1.0%. This uncertainty is dominated by the uncertainties of the throat diameter and the propellant flow rates. The butane data that is presented here is from an older set of experiments and the uncertainty in the c* measurements for this data set is approximately 2.0%.

Figure 5 shows a comparison of several of the element types at a nominal pressure of 3.44 MPa (500 psi) except for elements #3 and #7 which were only evaluated at a pressure of about 1.72 MPa (250 psi). The converging element (#11) produced the highest c* efficiency. Qualitatively, one would expect that this element would have a high heat load due to the mixing and burning that likely occurs within the cup. This was confirmed by the heat markings seen on the element. However, the heat loads were not high enough to damage the element. The c* efficiency increases slightly with increasing MR, i.e., with the resulting increased oxidizer injection velocity. This injector has shown no signs of chug instability. In fact, very little combustion noise is seen in the data with the standard deviation of chamber pressure less than 0.7% of the mean chamber pressure. This can be seen in Figure 6 which is a plot of a typical pressure trace from the experiments.

The pre-filming element (#13) which has a relatively small inside diameter also showed excellent combustion performance, but resulted in a much higher pressure drop than the converging element design (#11). Figure 7 shows the measured gas and liquid side injector pressure drops, normalized by the chamber pressure for six of the elements in cold-flow and hot-fire conditions. The pressure drop for injector #13 was much higher than the cold-flow pressure drop. It is believed that combustion was occurring within the element which caused significant propellant acceleration and pressure drop.

The pre-filming element (#7) demonstrated lower performance than the converging design. However, this element showed the most heat marking. In fact, the marking was so severe, that testing was not conducted at chamber pressures exceeding 3.44 MPa (500 psi). Both of these pre-filming injectors experienced a 200 Hz chamber pressure oscillation.

Figure 8 is a comparison of the measured cold flow mixing efficiencies and the hot-fire c* performance using two different scaling methodologies with butane as the fuel. The original scaling between hot-fire (butane/GOX) and cold-flow (water/gN2) conditions was based upon typical momentum ratio scaling used for shear coaxial injectors. The procedure was to match the liquid injection velocity and the gas density to the hot fire conditions, then to adjust the gas flowrate to match the gas-to-liquid momentum ratio. As can be seen by the dashed line in Figure 8, this methodology resulted in a very poor correlation between the cold flow and the hot fire results. Further investigation indicated that the gas-to-liquid momentum ratio might not be the appropriate scaling parameter for gas-centered swirl injectors. A revised scaling approach was then adopted which involved matching the gas density and injection velocity to the hot-fire conditions and adjusting the water flowrate to match the absolute momentum difference between the gas and liquid flows, as shown by the solid line in Figure 8. This approach resulted in a much better correlation between the cold flow and hot fire results, and demonstrates the importance of understanding the proper physical mechanisms when scaling between cold flow and hot fire evaluations.

Although mixing efficiency is only partially related to c* performance, there is a distinct correlation between the hot fire and the cold flow data. Note that the cold-flow mixing efficiency was measured 5.08 cm downstream from the injector exit, while the hot fire experiments were conducted with a 20.32 cm long chamber. The longer chamber provides more time for mixing to occur, which improves performance. In the limit of an infinitely long chamber with no losses all of the injectors would perform

at 100% efficiency. Thus the correlation between cold flow and hot fire evaluations should depend on the hot fire combustion chamber length.

After this initial screening, three more diverging element designs were examined. These designs were labeled 12A, 12B, and 12D. Due to facility changes, these three new diverging designs were evaluated with RP-1 instead of Butane. The results of these evaluations are shown in Figure 9. Note that design 12D had a c* efficiency in excess of 95%. This is approximately 5% higher than that of 12A and 12B. Figure 10 shows c* efficiency results from RP-1 testing for injector 11. As can be seen from comparing these results with those in Figure 5, the c* efficiency was approximately the same for RP-1 as it was for butane.

In order to demonstrate the capability of the facility to perform accurate combustion performance measurements, additional evaluations were performed with injector 11 using JP-7, JP-8, and JP-10 as fuels. The densities of these fuels varies by nearly a factor of two, and their viscosities vary by an order of magnitude, as indicated in table 3. The results of the combustion performance evaluations are shown in Figure 11. The results confirm the fuels performed nearly the same as predicted. The results also show that, despite the difference in densities and viscosities, injector #11 is not only highly performing but relatively insensitive to fuel type, as well as being relatively insensitive to chamber pressure for the two pressures examined.

ANALYSIS OF THE RESULTS

In an effort to better understand the effect of injector design and operating conditions on combustion performance, an analysis of the film breakup process was conducted. The cold-flow results indicate that the best performing injectors are the ones in which the swirling liquid film is completely stripped and entrained into the gas flow. Incomplete stripping of the liquid film inside the cup region results in the remaining film being thrown radially outward away from the central gas core, resulting in poor mixing. This is supported by the correlation between cold-flow mixing efficiency and hot-fire c* performance, to be shown below. A search of the literature revealed a liquid stripping correlation used for shear coaxial injectors originally proposed by Mayer (9). The breakup rate, or rate of mass removal from the liquid core (per unit area) is given by;

$$\dot{m}_b = C_1 \left[\frac{\mathbf{m}_l (\mathbf{r}_g V_r^2)^2}{\mathbf{s}_l / \mathbf{r}_l} \right]^{1/3} \qquad (2)$$

where V_r is the relative velocity between the gas and liquid streams, and C_1 is an empirically determined constant. In a first order analysis, one could calculate the breakup time as;

$$t_b = \frac{\dot{m}_l}{\dot{m}_b P V_l} \qquad (3)$$

where "P" is the perimeter of the contact area between the liquid and gas phase (P=πD) and V_l is the axial component of the liquid film velocity inside the cup region. This would be the time to fully strip the liquid film assuming that the flow conditions inside the cup region are constant in the axial direction. The residence time of the film can be calculated by: $t_r = \frac{L}{V_l}$ where "L" it the length of the cup, or the contact length between the gas and liquid phases. Since the mass flowrate of the thin liquid film is approximately equal to: $\dot{m}_f = \mathbf{r}_l V_l \mathbf{p} D \mathbf{t}_f$, where τ_f is the thickness of the swirling liquid film, the ratio of the film residence time to the breakup time (t_r/t_b) can be expressed as;

$$\frac{t_r}{t_b} = \frac{C_1 L}{\mathbf{t}_f} \left[\frac{\mathbf{m}_l}{\mathbf{s}_l} \left(\frac{\mathbf{r}_g}{\mathbf{r}_l} \right)^2 \frac{(V_g - V_l)^4}{V_l^3} \right]^{1/3} \qquad (4)$$

It is hypothesized that when the ratio of t_r/t_b is increased, the mixing efficiency or c* performance should also increase. The key parameter in the breakup rate is the relative velocity, V_r, which is equal to $(V_g - V_l)$. In calculating V_r we have used the liquid film axial velocity, V_l, calculated from inviscid flow theory, which yields an average film velocity (10). Since the bulk gas velocity in the cup region is roughly an order of magnitude larger than the film velocity, one might speculate that V_l has only a small effect on relative velocity. Using the "bulk flow" or average gas velocity inside the cup region produced only a very weak correlation between the measured hot fire performance and the film-stripping analysis described above. Further cold flow investigation revealed that the axial velocity profiles at the exit-plane of the injectors were not plug-flow for many of the diverging element designs. It is believed that a more appropriate gas velocity to use in the film-stripping

6

correlation would be the gas velocity at the gas-liquid interface.

In an effort to understand the potentially complex flowfield inside the cup region of the injectors studied here, a commercial CFD code (Fluent 6.1) was used to provide simulations of the gas flow through the injectors without the liquid circuit flowing. Several of the injector geometries were studied in a 2D axi-symmetric configuration with the computational domain extending from the gas inlet fitting in the injector manifold out into a small dump chamber. The simulations were designed to match the cold-flow conditions listed in Table 1, therefore the flow was modeled as a steady-state, compressible ideal gas (N_2) using a mass-flow inlet boundary for the inlet hole and static pressure boundaries for the dump chamber. A realizable k-e turbulence model was used with inlet turbulent kinetic energy and length scale profiles provided by experimental velocity measurements conducted in the cold-flow facility. Approximately 30,000 computational cells were ultimately used which was found to provide a grid-independent solution. A typical grid (injector 11) is shown in Figure 12.

Contour plots of axial velocity near the exit of the injector are shown in Figure 13 for injectors 5 and 11. As expected, injector 11 maintains a relatively uniform velocity profile throughout the injector with only a very small recirculation zone just downstream of the injector contraction. Injector 5 on the other hand reveals a very large recirculation zone in the cup region with a very low velocity near the injector wall where the liquid film would be located. The reattachment point for the flow appears to occur very near the exit of the injector. The simulations demonstrate the sensitivity of the flowfield to injector geometry and the need for a local gas velocity in the breakup rate correlation (Eq. 4) as opposed to a bulk-flow velocity.

In an effort to validate the CFD simulations in regards to the gas velocity near the injector wall, cold flow axial velocity profiles were measured for each of the injector types without the liquid circuit flowing. This was accomplished by seeding the gas flow upstream of the injector with a fine mist of water droplets in the size range of 1 to 10 μm. Droplet size and velocities were measured with the phase Doppler interferometer at an axial location of 2 mm from the injector face. Gas velocity was estimated by extrapolating the size-velocity relationship to the limit of zero size.

Figure 14 shows the experimentally measured mean (time averaged) axial velocity for injectors 5 and 11 along with the CFD simulations. The results validate the ability of the CFD code to reproduce the mean velocity field of the two injectors compared here.

Interface velocities for each injector was estimated by taking the experimentally measured gas-phase mean axial velocity at one film thickness from the wall. The film thickness was calculated using inviscid flow theory (10). The dashed lines in Figure 14 show the location of the estimated gas-liquid interface for injectors 5 and 11. Table 2 provides bulk-flow velocity, measured interface velocity and calculated film thickness for each of the injectors. The gas velocity at the film interface for the diverging element designs (nos. 3, 5, and 12) was found to be significantly lower than the bulk flow velocity due to flow separation in the expansion region of the cup as was observed in the CFD simulations for injector 5.

Using the gas velocity at the film interface, the correlating parameter (t_r/t_b) was calculated for the GOX/butane hot-fire conditions, and is presented in Figure 15 as a function of the measured c* efficiency. Although there is a significant degree of scatter in the plot, a fairly strong correlation can still be seen. The constant, C_1, in Eq. 4 was determined to be 0.01177 by setting the correlating parameter to be equal to 1.0 at a c* efficiency of 100%. This is somewhat arbitrary, but is based upon the hypothesis that combustion efficiency should be maximized when the ratio of residence time to breakup time is greater than or equal to 1.0.

The coefficient of determination, R^2, of the first order fit in Figure 15 was 0.71. Figure 16 is a plot of the correlating parameter versus c* efficiency for injectors 5, 11 and the 12 using RP-1 and JP-10 as fuels. The curve fit line in the plot in Figure 16 is the same as that from the Butane data (Fig. 15). With the possible exception of injector 5, Figure 16 demonstrates the ability of the correlating parameter to capture both the geometrical effects of the 12-series injectors and also the effect of fuel type. The results for injector 5 may be questionable because of the 200 Hz instability for this injector that was evident during the tests.

The effect of fuel type is better isolated from other effects such as gas velocity and density in Figure 17. Whereas Figure 16 contains all mixture ratios and chamber pressures, Figure 17 extracts data for a fixed injector type #11, a fixed nominal chamber pressure of 3.3MPa, and a fixed mixture ratio of 2.5. For each of the runs, the measured chamber pressure

7

and propellant flowrates were used along with the corresponding ambient condition fuel properties from Table 3 to calculate the value of the correlating parameter. The actual fuel temperature at the gas-liquid interface is unknown due to the possibility of combustion occurring inside the injector, therefore the fuel properties at the nominal inlet temperature of 298K are used as a basis for comparison. The relationship between c* and the correlating parameter from the first order curve fit in Figure 15 was used to predict c* for each of the test cases. Figure 17 shows a plot of the predicted c* versus the measured c* efficiency for each test case. Figure 17 shows that the fuel density and viscosity play a small but measurable role in combustion performance. The higher viscosity of JP-10 results in an increase in the stripping rate as given by Eq. 2. Also, the higher density of JP-10 results in a lower liquid film velocity and hence an increase in residence time and relative velocity in the cup region of the injector. Both factors result in an increase in the correlating parameter as well as combustion performance. In order to isolate the effects of liquid fuel properties from the gas properties and injector geometry, Equation 4 can be simplified by assuming that the liquid velocity in the numerator is negligible compared to the gas velocity and replacing velocity by $\dot{m}/\rho A$ for both the gas and liquid velocities. The result is Equation 5 which isolates the effect of the liquid fuel properties for a given injector geometry and OF ratio.

$$\frac{t_r}{t_b} = \frac{C_1 L}{t_f}\left[\frac{A_l^3}{A_g^4}\frac{\mathbf{m}_l \mathbf{r}_l}{\mathbf{s}_l}\frac{1}{\mathbf{r}_g^2}\frac{\dot{m}_g^4}{\dot{m}_l^3}\right]^{1/3} \qquad (5)$$

The last column in Table 3 contains the overall effect of the liquid fuel properties, $\mathbf{m}_l \mathbf{r}_l / \mathbf{s}_l$ from Eq. 5.

It is important to point out that the relatively wide variation in fuel properties studied here results in only a small variation in combustion performance compared to the strong effect of injector geometry on performance as shown in Fig. 15.

Finally, it may be observed that many of the chamber pressures achieved in the hot fire evaluations in fact exceeded the critical pressure of the respective fuels, yet the correlation parameter still captures the effects of fuel and injector type. Supercritical pressures potentially cause effects such as reducing the surface tension to zero which could invalidate the physical basis of Eq. 4. However, absorption and diffusion of gaseous oxygen into the fuels is known to significantly increase the critical pressure of the mixture. Phase equilibrium calcula-

tions of butane/oxygen mixtures reveal that the critical mixing pressure could be as high as 20 MPa, whereas most of the hot fire chamber pressures did not exceed 5 MPa. Therefore it may be expected with reasonable confidence that the mixtures were sub-critical, surface tension existed, and the physical basis of Eq. 4 remains sound.

SUMMARY

Design guidelines are being developed for gas-centered hydrocarbon swirl injectors. Three basic element concepts have been identified. A set of parametric injection elements has been designed in an effort to identify key design features and acceptable parameter values. Detailed cold-flow testing was performed on each of the elements with the goal of identifying unique injector characteristics. The cold flow data showed that the internal injector geometry played a key role in the measured mass distributions, mixture ratio distributions and atomization characteristics. Cold-flow CFD simulations were performed on several of the injector geometries and revealed unique internal flow features such as flow separation and recirculation which was found to have a large impact on injector performance.

Extensive hot-fire data was also collected with the same injectors used in the cold-flow phase of the program. The injectors were tested over a range of chamber pressures and mixture ratios and with a variety of hydrocarbon fuels. Within the range of fuels studied, it has been found that the converging element injector #11 is both high performing and relatively independent of fuel selection. The effect of injector geometry on the spray patterns and mixing uniformity observed in the cold-flow experiments was also observed in the hot-fire-results in the form of combustion performance. An increase in the cold-flow mixing uniformity resulted in an increase in combustion performance.

A film-stripping correlation developed for shear-coaxial injectors has been used to estimate the stripping rate of the liquid film inside the injector cup. The correlation takes into account both fluid property effects as well as injector geometry effects. The hot-fire performance data correlates reasonably well with the film-stripping correlation over a broad range of injector designs and a significant variation in fuel properties. The correlation also reveals an important parameter for injector scaling between cold-flow and hot-fire, which is the relative velocity between the liquid film and gas stream in the injector post.

8

REFERENCES

1. Lefebvre, A.; <u>Atomization and Sprays</u>. Hemisphere Publishing Corp, 1989.

2. Doumas, M. and Laster, R.; "Liquid-Film Properties for Centrifugal Spray Nozzles", *Chemical Engineering Progress*, Vol. 49, No. 10, Oct. 1953.

3. Muss, J.A., Johnson, C.W., Cheng, G.C., and Cohn, R.K. "Numerical Cold Flow and Combustion Characterization of Swirl Coaxial Injectors." AIAA 2003-0125, 41st AIAA Aerospace Sciences Meetings and Exhibit, Reno, NV, 6-9 Jan 2003.

4. Cheng, G.C., Davis, R.R., Johnson, C.W., Muss, J.A., Greisen, D.A., Cohn, R.K., "Development of GOX-Kerosene Swirl Coaxial Inector Technology". AIAA 2003-4751 39th AIAA Joint Propulsion Conference and Exhibit, Huntsville, AL, 20-23, July, 2003.

5. P. A. Strakey, D. G. Talley, L. K. Tseng and K. I. Miner, "The Effects Of LOX Post Biasing On SSME Injector Wall Compatibility", *Journal of Propulsion and Power*, Vol. 18, No. 2, March-April 2002.

6. Nurick, W. H., "Analysis of Sprays from Rocket Engine Injectors", *Journal of Spacecraft*, Vol. 8, No. 7, July, 1971, pp. 796-798.

7. Cohn, R.K., Strakey, P.A., Bates, R.W., Talley, D.G., Muss, J.A. and Johnson, C.W., "Swirl Coaxial Injector Development", AIAA 2003-0124, 41st AIAA Aerospace Sciences Meeting and Exhibit, Reno, NV, 6-9 Jan., 2003.

8. Cohn, R.K., Danczyk, S.A. and Bates, R.W., "A Comparison of the Performance of Hydrocarbon Fuel in an Uni-element Combustor", AIAA 2003-4752, 39th AIAA Joint Propulsion Conference and Exhibit, Huntsville, AL, 20-23, July, 2003.

9. Mayer, E., "Theory of Liquid Atomization in High Velocity Gas Streams", *ARS J.*, Vol. 31, pp. 1783-1785, 1961.

10. Yule, A.J. and Chinn, J.J., "Swirl Atomizer Flow: Classical Inviscid Theory Revisited",

Presented at: The 6th International Conference on Liquid Atomization and Spray Systems, ICLASS-94, Rouen, France, July, pp. 334-341, 1994.

Test (Hot-Fire or Cold-Flow)	Pc (MPa)	Fvac (kN)	$\dot{m}^{Gas}$ (kg/s)	$\dot{m}^{Liq}$ (kg/s)	V^{Gas} (m/s)	V^{Liq} (m/s)	$\dot{m}V^{Gas} - \dot{m}V^{Liq}$	V^{Gas}/V^{Liq}	MR
Butane/GOX	1.72	1.48	0.078	0.028	43.3	14.1	2.99	3.1	2.8
H₂O/N₂	1.97	NA	0.078	0.036	43.3	10.8	2.99	4.0	2.1

Table 1: Comparison of element operating conditions, hot fire to cold flow (hot fire MR=2.8)

Injector	Gas Bulk Velocity (m/s)	Gas Interface Velocity (m/s)	Film Axial Velocity (m/s)	Relative Velocity (m/s)	Film Thickness (μm)
3	12	1.5	3.2	1.7	193
5	51	15	5.4	9.6	247
7	43	22	3.5	18.5	332
11	65	59	4.9	51.1	295
12	83	25	6.4	18.6	256
12A	83	25	6.4	18.6	256
12B	83	25	6.4	18.6	256
12D	127	64	7.3	56.7	280
13	157	79	7.2	71.8	322

Table 2: Gas and liquid properties in cup region. Pc=1.97 MPa, N₂=0.078 kg/s, H₂O=0.036 kg/s

Fuel	Density (kg/m³)	Viscosity (N s/m²)	Surface Tension (N/m)	$\dfrac{\dot{m}_l r_l}{s_l}$
Butane	579	1.68e-4	1.2e-2	8.11
RP-1	806	7.70e-4	2.8e-2	22.2
JP-10	929	3.50e-3	3.0e-2	108.4

Table 3: Properties of selected hydrocarbon fuels @ 298K and 0.1 MPa

_____
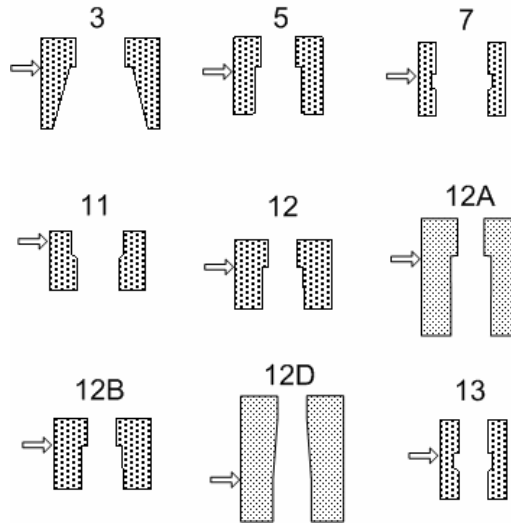
Figure 1 : Schematic drawings of the nine elements tested. Gas enters from the top and the location of the tangential liquid inlets are shown by arrows.
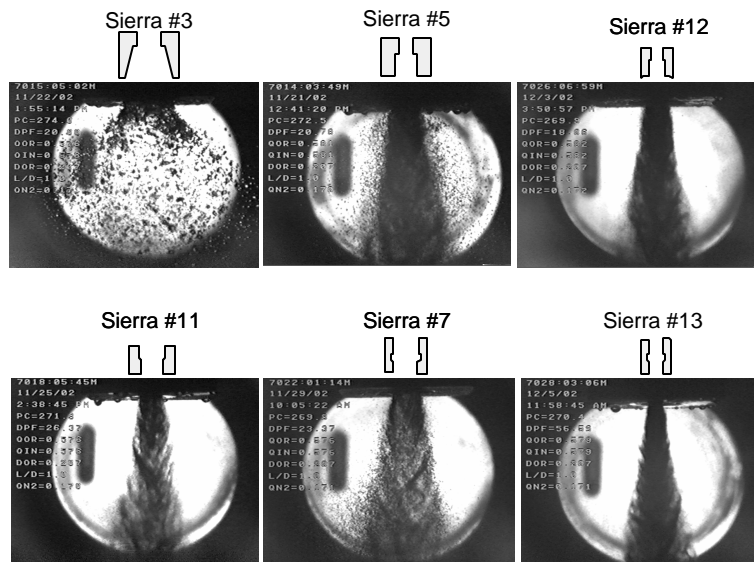
Figure 2: Strobe Back-Lit Images of Six El ement Types, Pc=1.97 MPa (271 psig)

Injector #3

Injector #5
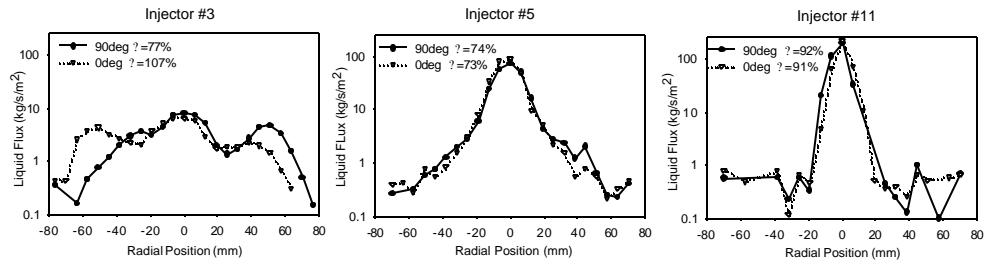
Injector #11

Figure 3: Corrected liquid mass flux profiles for injectors 3, 5 and 11 at an axial location of 5.08 cm and a chamber pressure of 1.97 MPa (271 psig) (see Table 1).
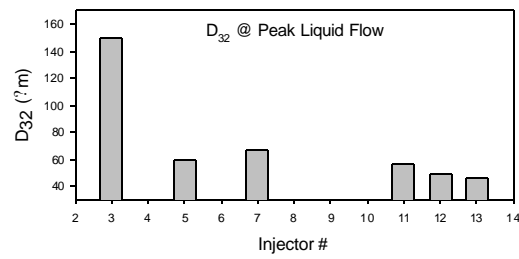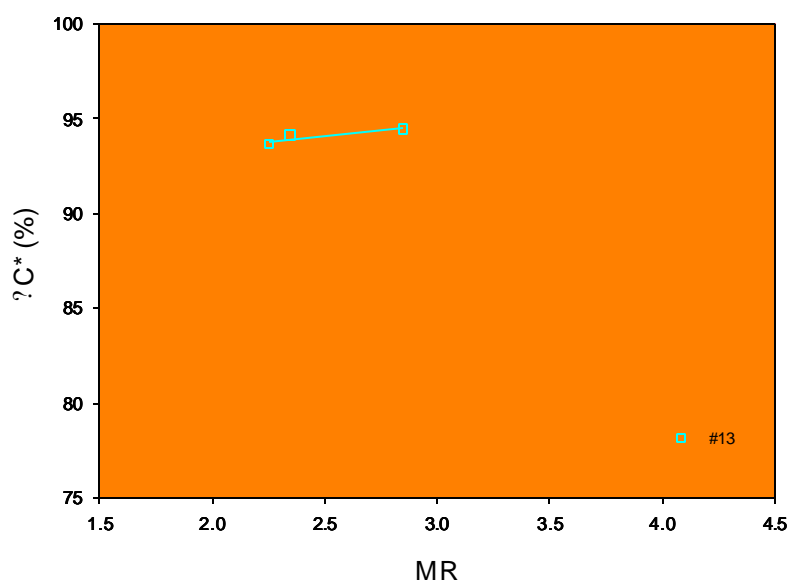
Figure 4: Sauter mean diameter at location of peak liquid flow.

Figure 5: C* efficiency versus MR for Diverging (#3, #5 and #12), Pre-filming (#7 and #13) and Converging (#11) Elements.   Pc ~ 1.72 to 3.42 MPa (250 to 500 psi), butane as fuel.
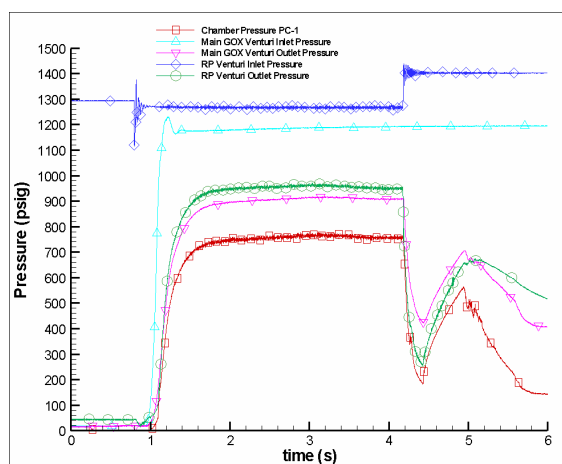
Figure 6: Sample pressure plot for Hydrocarbon fuel testing.
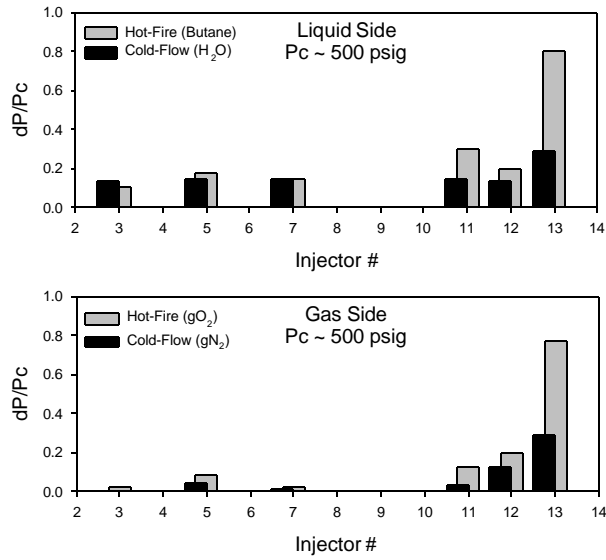
Figure 7: Hot-fire and cold-flow pressure Drop Data (dP/Pc) for Liquid and Gas Sides
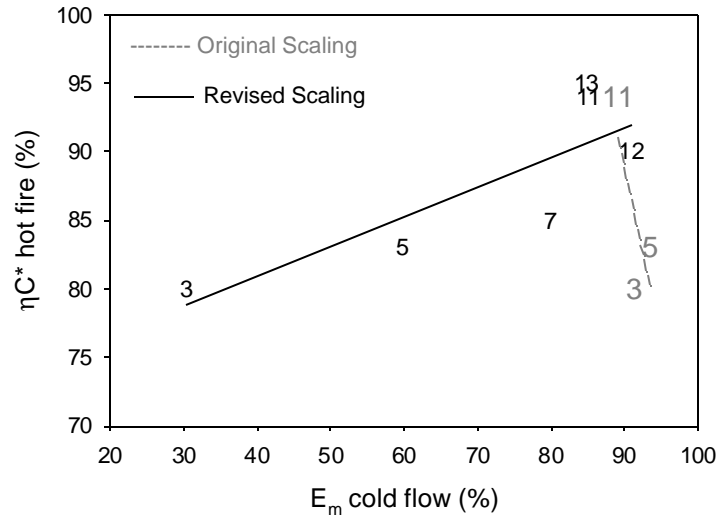
Figure 8: Correlation between hot-fire c* efficiency (MR=2.8, Pc=1.37 to 3.42 MPa (200 to 500 psia)) and cold-flow mixing efficiency (Pc=1.97 MPa (271 psig)) for six of the injector designs.

14
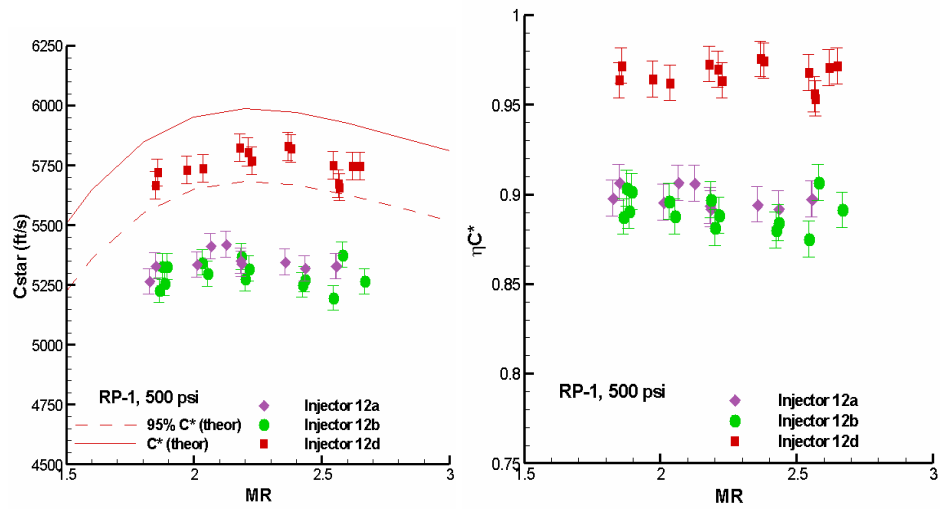
Figure 9: c* (a) and c* efficiency (b) for 3 different diverging injectors .
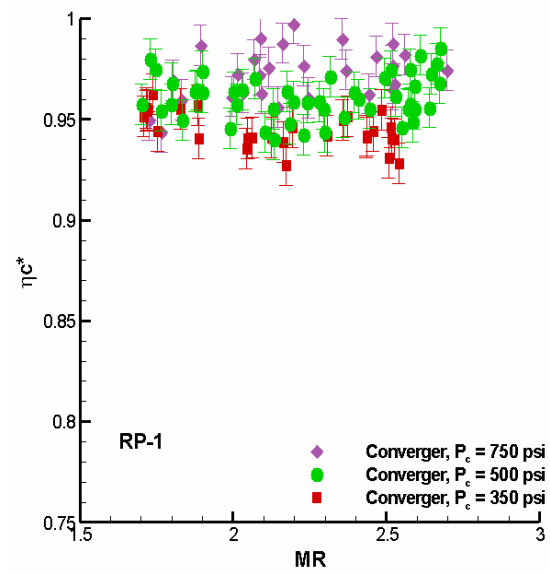
Figure 10: c* efficiency for RP-1 with Injector 11.
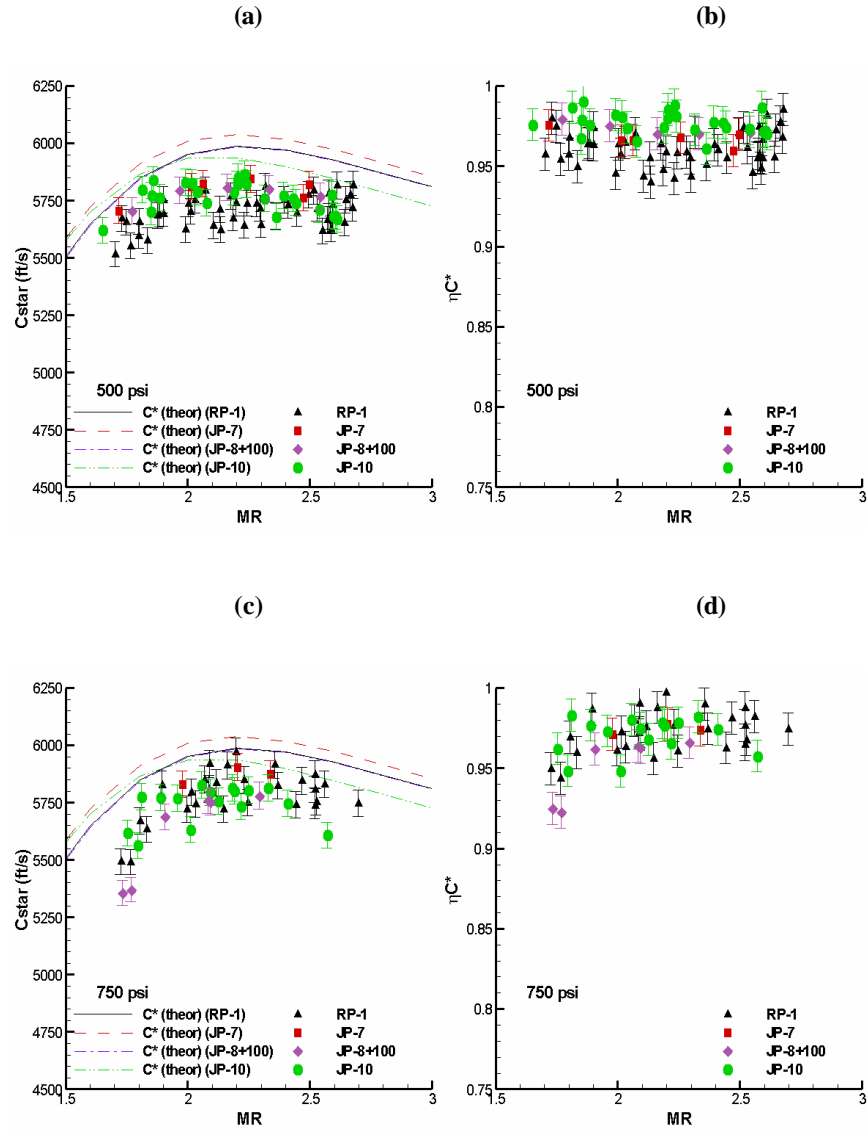
Figure 11: Performance of Injector 11 (converging injector) with a variety of hydrocarbon fuels. (a) c* for 3.42 MPa (500 psi). (b) C* efficiency for 3.42 MPa. (c) c* for 5.15 MPa (750 psi). (d) c* efficiency for 5.15 MPa.

16
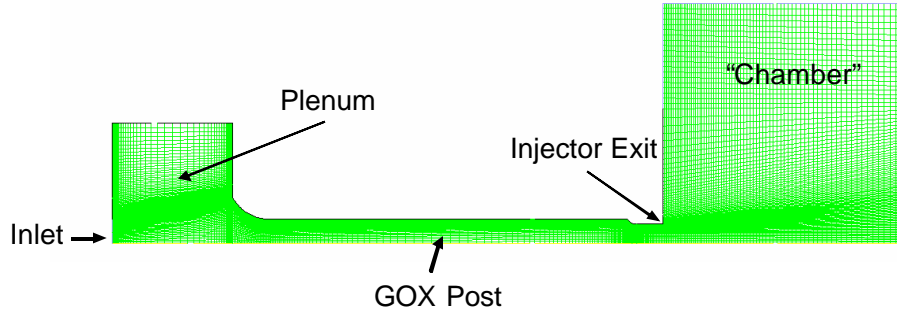
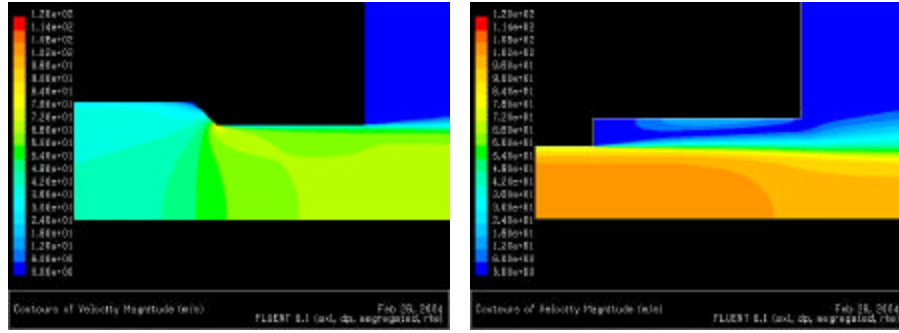**Figure 12: Typical grid structure for the CFD simulations (injector 11).**

Figure 13: Contours of velocity magnitude for injector 11 (left) and injector 5 (right) for the cold-flow conditions listed in Table 1. Flow is from left to right.
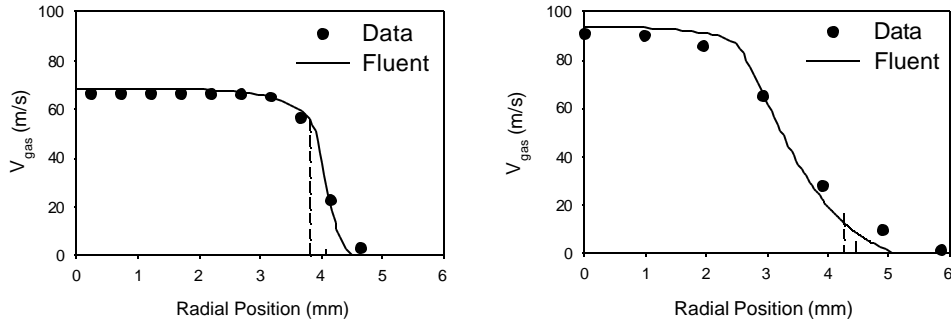

Figure 14: Comparison of CFD calculations and experimental measurements for mean velocity for injector 11 (left) and injector 5 (right) for the cold-flow conditions listed in Table 1 at an axial location of 2 mm from the injector face. Dashed lines indicate estimated location of the gas-liquid interface.
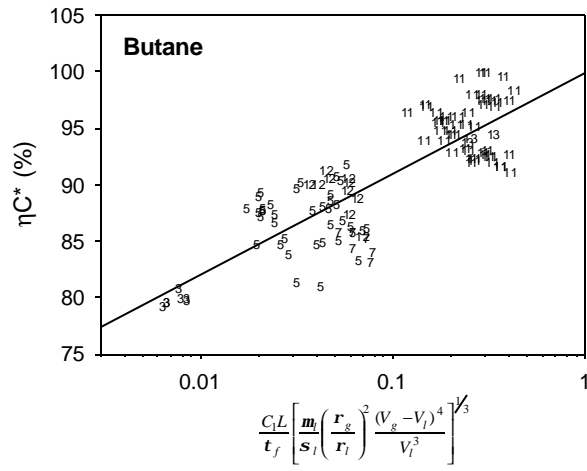
Figure 15: C* versus correlating parameter for all injectors (Butane data) using the interface velocity for gas side. Pc=1.3 to 6.53 MPa (190 to 950 psia), MR=1.8 to 4.1 and chamber length of 17.8 to 20.3 cm.
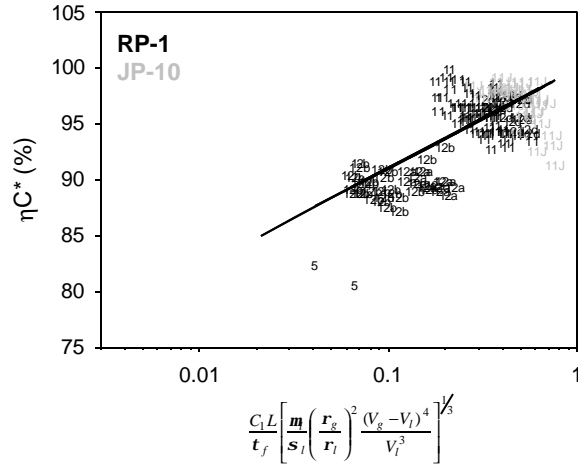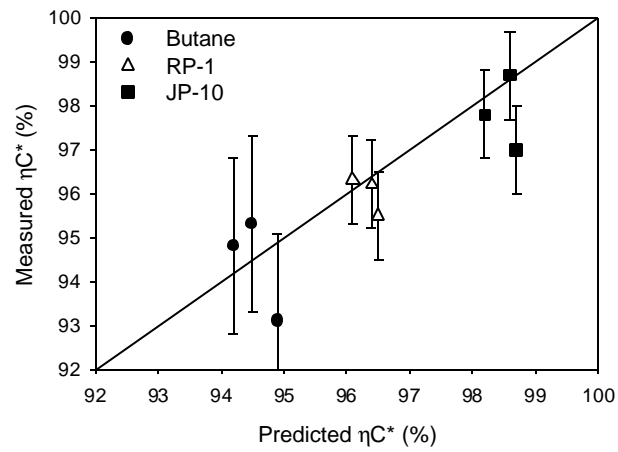

Figure 16: C* versus correlating parameter for injectors 5,11,12*(RP-1 and JP-10) using the interface velocity for gas side. Pc=1.49 to 5.36 MPa (217 to 780 psia), MR=1.5 to 5.0 and chamber length of 20.3 cm.

Figure 17: Predicted versus measured C* efficiency for Butane, RP-1 and JP-10 with injector #11. Pc=3.07 to 3.70 MPa (447 to 539 psig), MR=2.4 to 2.6.